Eur. Phys. J. A **9**, 313–326 (2000)

THE EUROPEAN PHYSICAL JOURNAL A

A phenomenological spin-orbit and nuclear potential for ^{208}Pb

G. Mairle[1] and P. Grabmayr[2,a]

[1] Universität Mannheim, Germany
[2] Physikalisches Institut, Universität Tübingen, Germany

Received: 12 September 2000
Communicated by P. Schuck

Abstract. A local, state-independent nuclear single-particle potential for ^{208}Pb was developed by suitably shaping the nuclear central term and the related spin-orbit term of Thomas type. The aim was to reproduce accurately the excitation energies of the known single-particle states in ^{207}Tl, ^{207}Pb, ^{209}Bi and ^{209}Pb as well as the recently observed dependence of the spin-orbit splittings on angular momentum ℓ and principal quantum number n. As result, a set of orthogonal proton and neutron wave functions was obtained which were used for a consistent reanalysis of proton and neutron single-particle transfer reactions on ^{208}Pb. The quality of the description of measured angular distributions is comparable with that obtained originally with individual "best fit" potentials. The resulting single-particle spectroscopic factors amount on the average to $S \approx 0.7$. Single-particle densities derived from these wave functions are in qualitative agreement with measured charge and mass densities for ^{208}Pb.

PACS. 21.60.Cs Shell model – 21.10.Jx Spectroscopic factors – 27.80.+w mass range 190-219 – 25.45.Hi Transfer reactions, ^{2}H induced

1 Introduction

On the occasion of the 50th anniversary of the nuclear shell model many publications and conference contributions have appreciated its success and have discussed its limitations [1,2]. Investigations of single-particle aspects of the double magic nucleus ^{208}Pb were the subject of numerous experiments in the last 40 years. Therefore this nucleus is one of the best studied cases with respect to the independent particle model. To date the experimental data base on the states of ^{208}Pb and the surrounding nuclei has reached a stable state. In general the analysis of the experimental data was performed within the single-particle shell model, however, based on different methods, inconsistent parameter sets and sometimes unnecessary simplifying assumptions. So far a consistent analysis considering all data simultaneously is still missing. On the other hand, principally the proper theoretical description of the atomic nucleus must be in the framework of a relativistic many-body theory —a task, which can be realized at present only for very light nuclei. The rigorous treatment must be relaxed for the heavier mass systems. For practical applications, however, such calculations of, *e.g.*, angular distributions, exceed present capabilities in computing or loose the desired precision due to the assumptions made. Limitations have to be applied to configuration space and shape of potentials or interactions.

It is the aim of the present investigation to derive a purely phenomenological mean-field potential for ^{208}Pb which is based on experimentally determined input only. With the smallest number of assumptions and constraints in construction it will secure a consistent description of all available data on single-particle properties of ^{207}Pb, ^{207}Tl, ^{209}Pb and ^{209}Bi.

In general, such single-particle states are described with phenomenological models. According to the ideas of the shell model, the Schrödinger equation must be solved with an appropriate central and with a suitable spin-orbit potential. For protons a Coulomb potential is added. In practice, calculations of reaction cross-sections or polarization variables, based on standard routines of DWBA codes usually rely on Woods-Saxon potentials of fixed geometry for the central part, a spin-orbit potential with an arbitrary coupling constant and a Coulomb potential of a uniformly charged sphere. The result is an individual, state-dependent central potential, because the depth must be adjusted separately for each level to reproduce the measured separation energy of a nucleon with quantum numbers n, ℓ and $\jmath$.

For the present analysis an eminent role is given to the spin-orbit partners, *i.e.* single-particle levels with fixed principal quantum number n and angular momentum ℓ, but opposite coupling of spin $s = 1/2$ to yield a total angular momentum $\jmath = \ell \pm 1/2$. These eigenstates have characteristic energies $E(n\ell\jmath)$. The energy difference of

[a] e-mail: grabmayr@pit.physik.uni-tuebingen.de

this pair of levels, the spin-orbit splitting

$$\varepsilon_{\rm so} = E(n\ell\jmath = \ell - 1/2) - E(n\ell\jmath = \ell + 1/2) \qquad (1)$$

clearly originates through details in shape and strength of the respective spin-orbit potential. In contrast, the central potential determines the single-particle energies $E(n\ell)$ which are not affected by the spin-orbit interaction.

In some models the strength of the spin-orbit potential must be adjusted to describe the individual observed spin-orbit splittings. One cannot expect [3,4] that the fine structure of the single-particle spectra with energies $E(n\ell\jmath)$ and the deduced dependence of $\varepsilon_{\rm so}$ on quantum numbers n and ℓ [5,6] can be described exactly by a central potential with simple parametrisation of Woods-Saxon type, which in addition must absorb the deficiencies of the Coulomb and spin-orbit potentials. A more rigorous method to search for state-independent shell model potentials for ^{208}Pb of Woods-Saxon plus spin-orbit potential of Thomas type has been applied among others by Bohr and Mottelson [3], Mahaux and Sartor [4], Rost [7], Blomquist and Wahlborn [8], and Bhattacharya [9]. Due to the simplicity of the models, the results are, of course, unsatisfactory as far as the agreement with measured single-particle energies, details of the spin-orbit splittings and the deduced shape of the spin-orbit potential is concerned.

Apart from these attempts of a phenomenological description on the basis of roughly parametrized single-particle central and spin-orbit potentials, numberless publications report on the derivation of shell model potentials from the nucleon-nucleon interaction and show the connections with nuclear densities [10,11]; others treat finite nuclei in relativistic mean-field models [12–17]. Particularly the spin-orbit potential and its relation to the two-body spin-orbit and tensor interaction has been the subject of many investigations [10,11,18–20]. In general these analyses aim at a principal understanding of the experimentally observed phenomena. They have the virtue of relying on basic ideas, but the comparison of the results with measured data has only qualitative character.

A typical result of those models is the fact that the relation between the mean-field central potential $V_{\rm N}(r)$ and the spin-orbit potential $V_{\rm so}(r, \ell s)$ is given by the Thomas form:

$$V_{\rm so}(r, \ell s) = -\frac{1}{2}\left(\frac{\hbar}{m_\pi c}\right)^2 \lambda \, \frac{1}{r}\frac{{\rm d}V_{\rm N}(r)}{{\rm d}r}\,(\ell \cdot \mathbf{s}) \qquad (2)$$

which is well known from atomic physics.

It is the aim of the present investigation to present a purely phenomenological model, which describes as accurately as possible the single-particle energies in ^{208}Pb and the systematic fine structure of the spin-orbit splittings. We try to use only measured results and avoid unnecessary model assumptions.

Many established spin-orbit doublets exist for the shell closure at ^{208}Pb. They are observed in the particle and the hole spectra of neutrons and protons with respect to ^{208}Pb, *i.e.* in the low-lying single-particle states of ^{207}Pb, ^{209}Pb, ^{207}Tl and ^{209}Bi.

The starting point of the present analysis is the systematic behaviour of the fine structure observed for nuclear spin-orbit splittings $\varepsilon_{\rm so}$ of nuclei in the vicinity of closed shells [5,6]. Besides the well-known $(2\ell + 1)$-proportionality of $\varepsilon_{\rm so}$, a $(1/n)$-dependence on the principal quantum number n has been found [5] at least for all observed states near the Fermi level, and a monotonous decrease with increasing mass number A.

The shapes of the potentials are described by a sum of cubic splines. This parametrization permits easy modifications of shapes and strengths of the central potential to reproduce the single-particle energies $E(n\ell)$ and of the spin-orbit potential to describe the spin-orbit splitting $\varepsilon_{\rm so}$. The only constraint in this procedure is eq. (2), the Thomas prescription, which connects the central and spin-orbit potential. This search was performed separately for protons and neutrons in ^{208}Pb.

The solution of the Schrödinger equation with these potentials for protons and neutrons with quantum numbers n, ℓ and $\jmath$ yields the desired single-particle energies and a set of orthogonal wave functions. Their validity can be tested by i) comparison of calculated spectroscopic quantities like spectroscopic factors with results of single-particle transfer reactions, and ii) comparison of single-particle densities with measured charge and mass densities.

In section 2 we recollect empirical data on single-particle energies and spin-orbit splittings, we describe the numerical procedure to shape the single-particle central and spin-orbit potentials in section 3, and we discuss the resulting effective potentials in section 4. Section 5 deals with a comparison of calculated and measured single-particle properties: single-particle spectra of ^{207}Pb, ^{207}Tl, ^{209}Pb and ^{209}Bi, spin-orbit splittings, spectroscopy of neutron and proton pick-up and stripping reactions on ^{208}Pb and single-particle densities. In section 6 we discuss the deduced spin-orbit potential in context with theoretical results derived form different model assumptions and give a conclusion in section 7.

2 Experimental data

Single-particle energies $E(n\ell\jmath)$ and spin-orbit splittings $\varepsilon_{\rm so}(n\ell)$ of protons and neutrons in ^{208}Pb were calculated from ground-state separation energies and excitation energies in ^{207}Tl, ^{207}Pb, ^{209}Bi and ^{209}Pb. The data were taken from the latest compilations of Nuclear Data Sheets [21, 22] which are based on results from single-particle transfer reactions on ^{208}Pb. These data are widely accepted in the literature and represent the basis of several theoretical investigations [4,7,9–13,20,23,24]. The proton and neutron energies $E(n\ell\jmath)$ and deduced spin-orbit splittings $\varepsilon_{\rm so}(n\ell)$ are listed in tables 1 and 2. The energies for protons in the $2f_{5/2}$, $3p_{1/2}$ and $3p_{3/2}$ shells are regarded to have in part considerable experimental errors; the same is true for neutrons in the $1h_{9/2}$, $1h_{11/2}$, $1i_{13/2}$, $2f_{5/2}$ and $2f_{7/2}$ shells. They were used with smaller weights in the fit procedures (see section 3). We note, that all energies are close to the Fermi energy and remember the fact

Table 1. Proton states in ^{207}Tl and ^{209}Bi (energies in MeV).

$n\ell j$	$E(n\ell j)$		$E(n\ell)$		$\varepsilon_{so}(n\ell)$		$\tilde{\varepsilon}_{\rm so}(n\ell)$	
	Exp.	Calc.	Exp.	Calc.	Exp.	Calc.	Exp.	Calc.
$1h_{9/2}$	−3.799	−3.903	−6.833	−6.705	5.562	5.504	1.011	1.001
$1h_{11/2}$	−9.361	−9.407						
$2d_{3/2}$	−8.364	−8.319	−9.163	−9.150	1.332	1.365	0.533	0.546
$2d_{5/2}$	−9.696	−9.684						
$2f_{5/2}$	−0.973	−0.730	−2.075	−2.145	1.929	2.057	0.551	0.588
$2f_{7/2}$	−2.902	−3.012						
$3p_{1/2}$	0.156	0.262	−0.402	−0.399	0.837	0.992	0.558	0.662
$3p_{3/2}$	−0.681	−0.730						
$3s_{1/2}$	−8.013	−8.017	−8.013	−8.017				

Table 2. Neutron states in ^{207}Pb and ^{209}Pb (energies in MeV).

$n\ell j$	$E(n\ell j)$		$E(n\ell)$		$\varepsilon_{so}(n\ell)$		$\tilde{\varepsilon}_{\rm so}(n\ell)$	
	Exp.	Calc.	Exp.	Calc.	Exp.	Calc.	Exp.	Calc.
$1h_{9/2}$	−11.4	−11.698	−14.1	−14.170	5.1	4.530	0.9	0.824
$1h_{11/2}$	−16.5	−16.229						
$1i_{11/2}$	−3.158	−3.341	−6.640	−6.722	6.466	6.279	0.995	0.966
$1i_{13/2}$	−9.624	−9.620						
$2f_{5/2}$	−8.081	−8.101	−9.245	−9.251	2.037	2.013	0.582	0.575
$2f_{7/2}$	−10.118	−10.113						
$2g_{7/2}$	−1.445	−1.371	−2.840	−2.796	2.511	2.566	0.558	0.570
$2g_{9/2}$	−3.956	−3.937						
$3p_{1/2}$	−7.368	−7.352	−7.967	−7.961	0.898	0.914	0.599	0.610
$3p_{3/2}$	−8.266	−8.266						
$3d_{3/2}$	−1.399	−1.259	−1.982	−1.934	0.971	1.124	0.389	0.450
$3d_{5/2}$	−2.370	−2.384						
$4s_{1/2}$	−1.905	−1.951	−1.905	−1.951				

that the single-particle energies of ^{208}Pb refer to different cores, when considering the $(A+1)$- and $(A-1)$-systems. For neutrons the core changes only by one mass unit out of $A = 208$. Therefore the solutions of the Schrödinger equation lead to negligible energy differences. However, for protons in addition the charge of the core changes by one charge unit out of only $Z = 82$ which yields energy shifts of $\Delta E = 240$ keV. This is important for the spin-orbit splitting of protons in the $1h$-shell (11/2-hole state in ^{207}Tl, 9/2-particle state in ^{209}Bi), where the difference of single-particle energies according to eq. (1) must be corrected by ΔE to obtain the net value of $\varepsilon_{\rm so}$.

The single-particle energies from tables 1 and 2 represent a considerable fraction of data on nuclear levels observed near the Fermi energy of closed shell nuclei. They were used for the investigation of nuclear spin-orbit splittings [5]. The graphical representation (fig. 1, top) presents the reduced spin-orbit splittings $\tilde{\varepsilon}_{\rm so}$=$\varepsilon_{\rm so}/((2\ell+1)/2)$ plotted *versus* mass number A. These quantities exhibit a pronounced dependence on the principal quantum number n and a monotonous decrease with mass number A. There are no evident differences for protons and neutrons and for particle-particle, particle-hole and hole-hole doublets. The spin-orbit splittings can be parametrized in terms of angular momentum ℓ, principal quantum number n and mass number A:

$$\varepsilon_{\rm so}(n\ell, A) = \frac{2\ell+1}{2}\,\frac{1}{n}\,kA^{-c} \qquad (3)$$

with parameters $k = 23.3$ MeV and $c = 0.58$.

The extracted A-dependence (fig. 1, bottom) as represented by the parameter c reflects a difference of the actual spin-orbit potential to that one which would be derived by the Thomas-prescription from a harmonic oscillator nuclear potential ($c = 2/3$). The $(1/n)$-dependence can be shown to result from a spin-orbit potential of unusual shape [6]. These relations are incorporated as starting point in the present investigation.

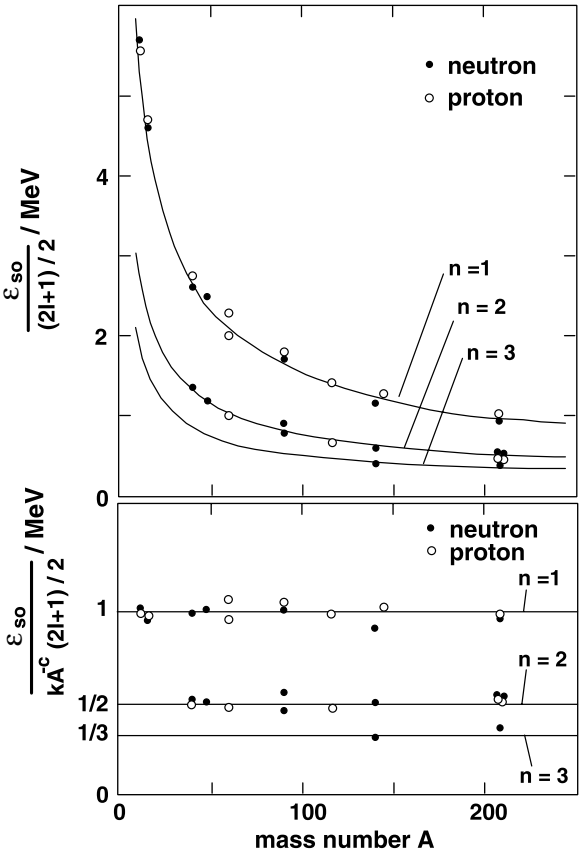

Fig. 1. Top: Measured spin-orbit splittings for protons (open circles) and neutrons (full circles) in the mass region between ^{12}C and ^{208}Pb after normalisation by $(2\ell{+}1)/2$. The data from tables 1 and 2 show a monotonous decrease with mass number A, which can be described by $f(A){=}kA^{-c}$ (eq. (3)) and a characteristic relation to the inverse of the principal quantum number n (full lines) Bottom: The further normalisation by $f(A)$ demonstrates the $(1/n)$-dependence more clearly.

3 The numerical procedure

The present investigation searches for unique state-independent local potentials for protons and neutrons. When inserted in the appropriate Schrödinger equation they must reproduce the single-particle energies of tables 1 and 2. This requirement includes the inherent fine structure of the single-particle spectra expressed by the spin-orbit splittings. The interaction of a nucleon with the residual nucleus shall be given in a purely phenomenological description by

$$V = V_{\rm C}(r) + V_{\rm N}(r) + V_{\rm so}(r, \ell s). \qquad (4)$$

Without essential model assumptions we use

a) a Coulomb-potential $V_{\rm C}(r)$ derived from the measured charge density of ^{208}Pb [25],
b) a nuclear potential $V_{\rm N}(r)$, the radial extent of which is estimated by the measured mass density [26],
c) a spin-orbit potential $V_{\rm so}(r, \ell s)$ of Thomas type (eq. (2)).

Separately for protons and neutrons, we shaped the potential wells $V_{\rm N}(r)$ and $V_{\rm so}(r)$ with the aim to minimize the differences between measured and calculated single-particle energies. Individual shaping of both potentials was achieved by a representation based on 20 natural (cubic) spline functions.

According to the potential decomposition of eq. (4) we calculated at first single-particle energies $E(n\ell)$ undisturbed by the spin-orbit interaction:

$$E(n\ell) = E(n\ell\jmath = \ell + 1/2) + \varepsilon_{\rm so}(n\ell)\,\frac{\ell}{(2\ell+1)}\,,$$
$$= E(n\ell\jmath = \ell - 1/2) - \varepsilon_{\rm so}(n\ell)\,\frac{(\ell+1)}{(2\ell+1)}\,. \qquad (5)$$

Equation (5) indicates the decoupled search procedure: $V_{\rm N}(r)$ must be optimized to reproduce the energies $E(n\ell)$ and $V_{\rm so}(r)$ must be optimized to reproduce the spin-orbit splittings $\varepsilon_{\rm so}(n\ell)$. However, both potentials cannot be varied independently, because $V_{\rm so}(r)$ is related to $V_{\rm N}(r)$ via the condition eq. (2).

The numerical procedure can be characterized as an iterated first-order perturbation calculation. We start with a suitable Woods-Saxon–type potential $V_{\rm N}^0(r)$, solve the Schrödinger equation for particles with quantum numbers $(n\ell)$ and obtain a set of wave functions $\Psi^0(n\ell)$ with radial part $R(n\ell)$ and energy eigenvalues $E^0(n\ell)$. Then we calculate the spin-orbit splittings in first-order perturbation theory:

$$\varepsilon_{\rm so} = \frac{(2\ell+1)}{2}\left(\frac{\hbar}{m_\pi c}\right)^2 \lambda \int_0^\infty \frac{1}{r}\frac{{\rm d}V_{\rm N}}{{\rm d}r}\; R^2(n\ell)\, r^2 {\rm d}r \qquad (6)$$

and modify the shape of $V_{\rm so}(r)$ until best agreement with measured values of $\varepsilon_{\rm so}(n\ell)$ was achieved. After that, the nuclear potential $V_{\rm N}(r)$ is reconstructed from $V_{\rm so}(r)$ by integration:

$$V_{\rm N}(r) = \int r\; V_{\rm so}(r)\, {\rm d}r. \qquad (7)$$

Application of first-order perturbation theory to the difference $\left(V_{\rm N}^0(r) - V_{\rm N}(r)\right)$ yielded the corrections $\Delta E(n\ell)$, which were minimized by suitable shaping of $V_{\rm N}(r)$. In turn, $V_{\rm so}(r)$ was generated according to eq. (2) and the shape improved to describe $\varepsilon_{\rm so}(n\ell)$. This procedure was continued until the potentials $V_{\rm N}^1(r)$ and $V_{\rm so}^1(r)$ reproduced all single-particle energies $E(n\ell)$ and spin-orbit splittings $\varepsilon_{\rm so}(n\ell)$, respectively. Solving the Schrödinger equation with these improved potentials provided a new set of wave functions $\Psi^1(n\ell)$, which enable the next step of perturbation calculations. This procedure was iterated until the deviations between calculated and measured values of $E(n\ell)$ and $\varepsilon_{\rm so}(n\ell)$ were of the order of the experimental errors. Final solution of the Schrödinger equation with the iterated potentials $V_{\rm N}^i(r)$ and $V_{\rm so}^i(r)$ yielded the eigenvalues $E(n\ell\jmath)$ which differed only insignificantly from the measured single-particle energies.

The compilations in tables 1 and 2 enable a quantitative comparison of calculated and measured values of

$E(n\ell)$, $E(n\ell j)$ and $\varepsilon_{\rm so}(n\ell)$. The r.m.s. deviations for both $E(n\ell)$ and $E(n\ell j)$ amount to $\Delta = 16$ keV for protons and to $\Delta = 25$ keV for neutrons. The differences can be further reduced in principle, but this seems to be not reasonable in view of the experimental errors.

4 The phenomenological potentials

4.1 The Coulomb potential

Following the concept to use measured input data in our analysis whenever possible and to avoid unnecessary model assumptions we did not use the standard Coulomb potential due to a uniformly charged sphere. Instead we applied a potential derived from the measured charge distribution [25] of ^{208}Pb in a parametrisation given by Eder and Oberhummer [27]. Small energy differences occurred (~ 10 keV), when we extracted the Coulomb potential in a spline representation directly from the measured charge density by applying the Maxwell equation in its integral form (Gauß's law). The potential of a charged sphere and that derived from the experimental data show significant differences at small radii. These differences lead to shifts in single-particle energies as large as 5 MeV. Usually these remarkably large deficiencies of the model potentials are tacitly absorbed in the nuclear (Woods-Saxon) potential.

4.2 The nuclear potentials

In fig. 2 the nuclear potentials $V_{\rm N}(r)$ for protons and neutrons are shown which represent the final result of the fitting procedure described in section 3. With these potentials a convincing description of the single-particle energies $E(n\ell)$ unperturbed by the spin-orbit interaction could be achieved and the complete calculation when including in addition the respective spin-orbit potential $V_{\rm so}(r)$ described in section 4.3 reproduces the measured energies $E(n\ell j)$ very well as can be demonstrated by the numbers of tables 1 and 2.

At first sight the potentials for neutrons and protons resemble Woods-Saxon–like wells with depths of $V_0 \approx -46$ MeV and $V_0 \approx -66$ MeV, radius parameters $r_0 = 1.25$ fm and $r_0 = 1.21$ fm, and large values for the diffusenesses $a_0 \approx 0.8$ fm and $a_0 \approx 1$ fm, respectively. However, deviations from a Woods-Saxon form factor are substantial. We see a minimum of the potentials around $r = 6$ fm (neutrons) and $r = 5.5$ fm (protons) and a maximum in the nuclear interior.

Details of the potential wells $V_{\rm N}(r)$ are well defined, because the density functions $R^2(n\ell)r^2$ of valence orbits probe the complete nuclear region. For protons a total of 11 maxima from the observed valence orbits $1h$, $2d$, $2f$, $3s$ and $3p$ contribute while 16 maxima from the $1h$, $1i$, $2f$, $2g$, $3p$, $3d$ and $4s$ neutron orbitals are relevant.

The shape of the nuclear potentials $V_{\rm N}(r)$ in fig. 2 are exclusively the result of the fitting procedure. Their characteristic features seem to be remarkable at first glance. In

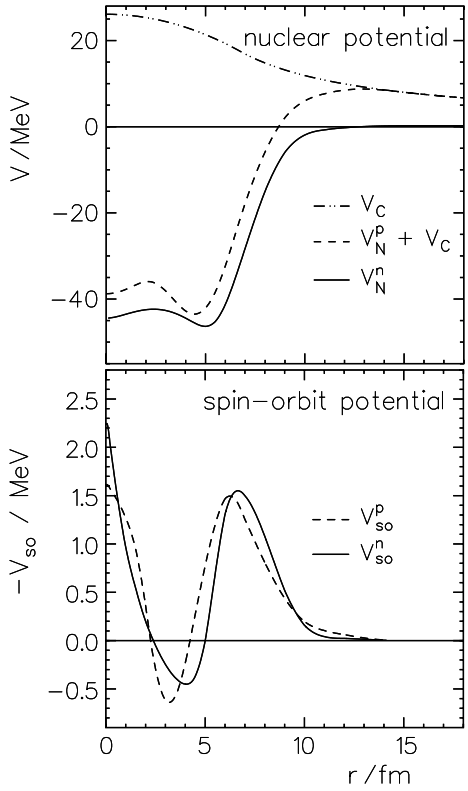

Fig. 2. State-independent nuclear potentials $V_{\rm N}(r)$ for neutrons and protons in ^{208}Pb including the Coulomb potential $V_{\rm C}(r)$ due to the measured charge distribution (top) and the corresponding spin-orbit potentials $V_{\rm so}(r)$ (bottom). The potentials are connected via the condition eq. (2) (Thomas form).

Fourier-Bessel analyses of scattering data [28], which represent an alternative method to vary the Woods-Saxon form factor, similar potentials have been found. Qualitatively the same structures occur in other quantum-mechanical many-body systems, *i.e.* in the self-consistent total potentials of metal clusters [23,29] like Na_{198}. The apparent similarity between our phenomenological potentials and those obtained from HF calculations on ^{208}Pb with extended Skyrme forces [23,30] shows that our results are presumably not fortuitous.

4.3 The spin-orbit potentials

The shapes of the final spin-orbit potentials for neutrons and protons are shown at the bottom of fig. 2. The characteristic maximum in the region of the nuclear surface is expected [3] for any spin-orbit potential of the type $V_{\rm so} \sim (\nabla\rho \times \mathbf{p})\cdot\mathbf{s}$ because the gradient of the nuclear density $\rho(r)$ in ^{208}Pb has its maximum around $r =$ 6-7 fm. Apart from this known feature the potentials exhibit their minima with negative values in the nuclear interior followed by an insignificant increase towards the nuclear center. These unexpected shapes are well determined by the maxima of the density functions $R^2(n\ell)r^2$ of the valence orbits as has been discussed for the nuclear potential.

Fitting the measured spin-orbit splittings $\varepsilon_{\rm so}$ within a procedure like the present one allows also to extract the strength λ of the potentials (eq. (6)). As a result, we obtained $\lambda = 0.547$ and $\lambda = 0.744$ for protons and neutrons, respectively. The potentials of fig. 2 include the respective λ. We notice that both potentials show almost the same strength in the vicinity of the nuclear surface, however they peak at slightly different radii. Equal strength, however, is a necessary condition for equal values of $\varepsilon_{\rm so}$ for neutrons and protons of the same quantum numbers n, ℓ. The different coupling strengths λ obviously compensate the inherent influences of the different strengths of the nuclear potential $V_{\rm N}(r)$ for protons and neutrons. Indeed, the ratio of volume-integrals for $V_{\rm N}(r)$ equals the inverse ratio of the strengths λ.

Because the spin-orbit potential, which describes the measured splittings $\tilde{\varepsilon}_{\rm so}(n\ell)$, and the nuclear potential, which in turn describes the energies $E(n\ell)$, are intimately connected by the constraints of eqs. (2) and (7), the minima of $V_{\rm so}(r)$ and the wiggles of $V_{\rm N}(r)$ are interdependent and their existence seems to be necessary. The strict correlation of both potentials represents the sole model assumption in our analysis. While this is widely accepted and discussed in the text books [3,31], it never has been applied in such a strict way to derive the shapes of potentials.

4.4 Single-particle energies

In fig. 3 the complete energy spectra $E(n\ell)$ and $E(n\ell j)$ are shown for protons and neutrons. The experimentally known region around the Fermi level $E_{\rm F}$ extends up to binding energies of about $E_{\rm B} = -11$ MeV including all fitted levels. In the remaining part of the spectra, the energetic position of the more tightly bound nucleons should be regarded as extrapolation.

The $1s_{1/2}$ levels occur at 36 MeV and 40 MeV for protons and neutrons being in qualitative agreement with results of Hartree-Fock calculations with non-local Skyrme forces [23,30] and of relativistic mean-field model calculations [12]. From fig. 3 we see that already the single-particle energies $E(n\ell)$ which are unperturbed by the spin-orbit interaction show shell structures. This seems to be obviously a common signature of quantum-mechanical fermion systems. When, in addition, the spin-orbit potential is included in the calculations, we obtain the typical shell gaps of nuclear systems and the familiar level sequence known from lighter nuclei. Several relativistic and nonrelativistic Hartree calculations, *e.g.* [26,32–35], cannot reproduce the single-particle energies and the spin-orbit splittings at the same time.

The present potentials $V_{\rm N}(r)$ and $V_{\rm so}(r)$ have the virtue to be state independent. They produce a complete set of single-particle energies and of orthogonal wave functions, but they are local. This has little importance in the region of weakly bound nucleons below the Fermi energy, where nonlocality effects are small, and effective masses were shown [23] to have values $m^*/m \simeq 1$. Our predictions for single-particle energies of deeply bound nucleons must be regarded, however, with care. Interestingly, theoretical predictions for such states starting from basic concepts like Hartree-Fock [23] and relativistic mean-field models [12] show qualitatively the same results. In principle, nonlocality corrections could have been included in the present analysis, but we decided to avoid the corresponding model assumptions in order to get a pure phenomenological description. As far as the spin-orbit interaction is concerned, a state-independent, non-local spin-orbit potential has been derived by Scheerbaum [20] with few model assumptions. We regard our predicted energies for deeply bound nucleons to be of minor importance, because their experimental observation seems to be impossible. A complete set of wave functions allows, however, the calculation of quantities like single-particle densities, which can be compared with experimental results and offers the possibility to test theoretical predictions for spin-orbit splittings, which are based on nuclear densities.

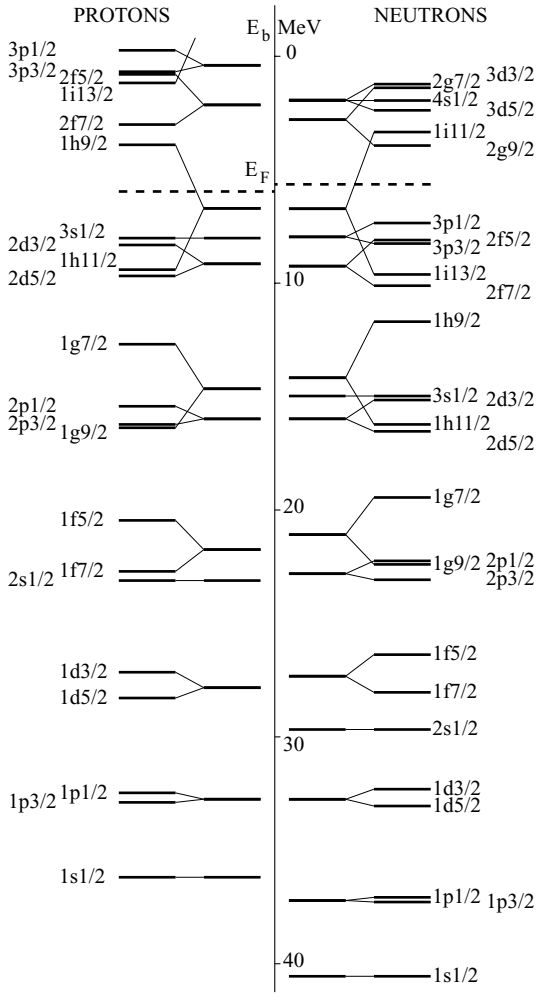

Fig. 3. Proton and neutron spectrum of ^{208}Pb calculated with potentials shown in fig. 2. The level schemes are given without and with spin-orbit splitting resulting in energies $E(n\ell)$ and $E(n\ell j)$, respectively. The experimentally known states are found around the Fermi energy $E_{\rm F}$ in the region with binding energies up to about $E_{\rm B} \approx -11$ MeV.

4.5 Spin-orbit splittings

The resulting absolute values $\varepsilon_{\rm so}$ of the spin-orbit splittings for protons and neutrons and the corresponding reduced values $\tilde{\varepsilon}_{\rm so} = \varepsilon_{\rm so}/((2\ell+1)/2)$ are compared to the experimental data in tables 1 and 2. The quality of the description of the fine structure of the spectra expressed by the dependence of $\varepsilon_{\rm so}$ on the principal quantum numbers n and ℓ (eq. (6)) is remarkable. We point out the fact, that the pronounced dependence of $\varepsilon_{\rm so}$ on n is hidden by the generally much stronger ℓ-dependence. The $(1/n)$-dependence however appears very clearly in the reduced splittings $\tilde{\varepsilon}_{\rm so}$. Particularly, the ratio $r = \tilde{\varepsilon}_{\rm so}(n=1)/\tilde{\varepsilon}_{\rm so}(n=2) \approx 2$ is achieved, which is experimentally well established for protons in the $1h$, $2d$ and $2f$ shells and for neutrons in the $1i$, $2f$ and $2g$ shells. But also the deviations from the strict $(1/n)$-dependence for neutrons and protons in the $3p$ shell are reproduced.

The application of other phenomenological spin-orbit potentials which have been used in the past does not reproduce the spectra. Simple-mindedly $\tilde{\varepsilon}_{\rm so}$ could be calculated with a spin-orbit potential derived from a harmonic oscillator nuclear potential $V_{\rm N}(r) = -V_0 + \frac{1}{2}m\omega^2 r^2$ according to the Thomas prescription (eq. (2)). This leads —independently of the radial wave functions $R(n\ell)$ used in the calculation of the perturbation matrix elements— to the result

$$\varepsilon_{\rm so} \ = (2\ell+1)/2 \cdot \lambda \cdot (\hbar\omega)^2/2m_\pi c^2 \qquad (8)$$

giving constant reduced splittings which are independent on the principal quantum number n at all, in contrast to the experimental findings.

The widely accepted procedure to derive the spin-orbit potential of Thomas type from a Woods-Saxon nuclear potential leads to the typical surface-peaked potential well and to $\tilde{\varepsilon}_{\rm so}(n=1)/\tilde{\varepsilon}_{\rm so}(n=2) \approx 1.4$. Thus, this type of potential cannot reproduce the measured $(1/n)$-dependence, *i.e.* the ratio 2.

Inspection of the radial distribution of the density functions $R^2(n\ell)r^2$ and the form factor of the spin-orbit potential discussed above shows a considerable overlap in the matrix element for the maximum of the $n=1$ functions ($1h$ for protons and $1i$ for neutrons) and the second maximum of the $n=2$ functions ($2d$, $2f$ for protons and $2f$, $2g$ for neutrons), respectively, with $V_{\rm so}(r)$. The first maximum of the $n=2$ functions, however, contributes only to a minor extent. Necessary for a further reduction of $\tilde{\varepsilon}_{\rm so}(n=2)$ are negative contributions to the matrix elements, which can be achieved only with negative values of $V_{\rm so}(r)$ in the region $r = 0.3$–0.4 fm. This idea has been outlined in ref. [6].

The result of the present calculations based on a free variation of the potential shapes exhibits exactly the desired behaviour (see fig. 2). The differences between proton and neutron spin-orbit potentials are characterized by a different radial extent. Certainly, this effect is caused by the different densities which are probed by protons and neutrons.

Inspection of the matrix element (eq. (6)) immediately shows, that the observed $(1/n)$-dependence of the reduced splittings $\varepsilon_{\rm so}$ cannot be an exact relation, because it depends on the overlap of the densities $R^2(n\ell)r^2$ with $V_{\rm so}(r)$. Indeed a constant value of $\tilde{\varepsilon}_{\rm so} \simeq 0.55$ can be calculated for $n=2$ states (*i.e.* $2p$, $2d$, $2f$ for protons and $2p$, $2d$, $2f$, $2g$ for neutrons), whereas we obtain a monotonous increase of $\tilde{\varepsilon}_{\rm so}$ for $n=1$ states, starting with $\tilde{\varepsilon}_{\rm so} = 0.14$ for $1p$ neutrons up to $\tilde{\varepsilon}_{\rm so} \approx 0.97$ for $1h$ protons and $1i$ neutrons. Obviously, the ratio $\tilde{\varepsilon}_{\rm so}(n=1)/\tilde{\varepsilon}_{\rm so}(n=2)$ has its maximum value of about 2 only around the Fermi energy and drops continually for more tightly bound nucleons. The same is true for unbound particles (see ref. [5]).

5 Comparison with spectroscopic quantities

The existence of a state-independent nuclear and spin-orbit potential and the corresponding complete set of wave functions for protons and for neutrons offers the possibility of a comprehensive and consistent reanalysis of spectroscopic data like spectroscopic factors of single-particle transfer reactions on ^{208}Pb, single-particle densities and rms radii.

In the past 40 years, the spectroscopic investigations of single-particle transfer reactions provided the empirical basis of the nuclear shell model. In early analyses of such reactions on closed-shell nuclei, the wave function of the transferred nucleon was calculated such as to reproduce the shell model expectation values, anticipating spectroscopic factors equal to unity. Later investigations have applied this procedure, although it has always been the subject of criticism, because the calculated differential cross-section changes by some 10% for a change of only 1% of the radius of the Woods-Saxon potential used to calculate the bound-state wave function, *e.g.*, for ^{208}Pb. Additional uncertainties arose from the fact that the bound-state potentials were determined individually for the different orbits $n\ell j$, that the spin-orbit potential was chosen highly arbitrarily and that a Coulomb potential remarkably different from reality was used in case of protons. For these reasons, such a determination of absolute spectroscopic factors is questionable, but also the calculation of relative spectroscopic factors should be taken with care.

In contrast to the previous analyses, the extraction of spectroscopic factors with single-particle wave functions determined with the present state-independent potentials seems to be unambiguous. The wave functions do not depend on an arbitrarily chosen potential radius. Their detailed behaviour over the complete nuclear region is well determined on the basis of the fitting procedure for the potential and there is no possibility to modify the absolute and the relative values of spectroscopic factors in the framework of a DWBA calculation.

The reanalysis of previous proton and neutron pick-up and stripping experiments on ^{208}Pb was performed in two steps. At first we tried to reproduce the spectroscopic factors using the parameters given in the original literature. In general, this was accomplished within 20% which is an acceptable error in view of the uncertainties i) to extract the numerical values of the cross-sections from the plots given in the papers and ii) to calculate DWBA

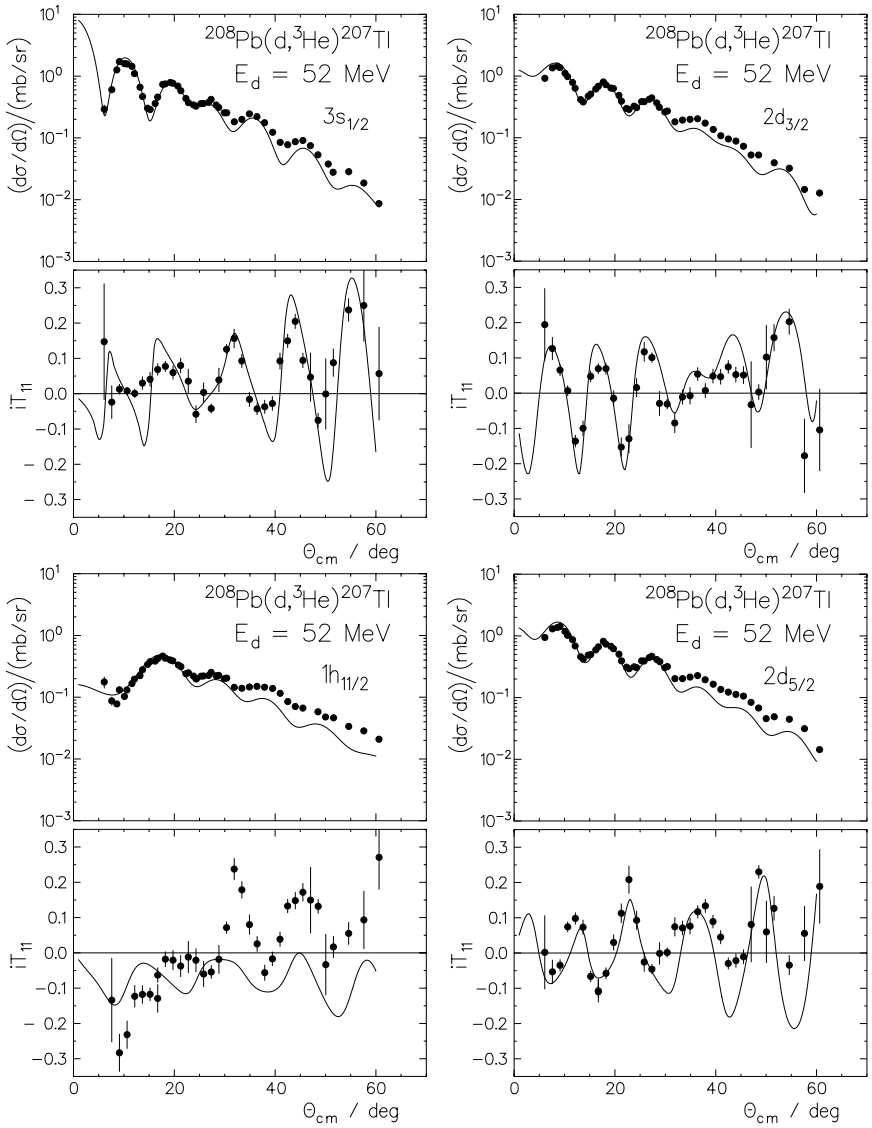

Fig. 4. Angular distributions of differential cross-sections and vector analyzing powers measured in the ^{208}Pb(d,^{3}He)^{207}Tl reaction at 52 MeV. The data from refs. [38,39] are compared to local, zero-range DWBA-predictions including bound-state wave functions, calculated in the state-independent potential described in section 4.

cross-sections with sometimes obviously incorrectly given input parameters and with the use of different DWBA codes. Then we repeated the DWBA calculations with the bound state potentials described in section 4. The code DWUCK4 [36] was employed in the local and zero-range approximation. For calculation of the distorted waves in the entrance and exit channels the original potentials have been used as cited in the respective papers.

5.1 The ^{208}Pb(d,^{3}He)^{207}Tl reaction

The proton pick-up reaction (d,^{3}He) has been originally investigated with a vector-polarized beam of 52 MeV deuterons by Grabmayr *et al.* [37–39]. The angular distributions of differential cross-sections and analyzing powers for proton hole states in the $3s_{1/2}$, $2d_{3/2}$, $1h_{11/2}$ and $2d_{5/2}$ shells are shown in fig. 4. The data are compared to local, zero-range DWBA-calculations with optical potentials

Table 3. Spectroscopic factors S from the ^{208}Pb(d,^{3}He)^{207}Tl reaction at 52 MeV.

E_x [a]	J^π [a]	S [b]	S [c]
0.0	$1/2^+$	0.80	0.64
0.351	$3/2^+$	0.87	0.68
1.348	$11/2^-$	0.89	0.43
1.683	$5/2^+$	0.61	0.44

[a] Energies in MeV, ref. [22].
[b] This work, data from refs. [38,39].
[c] References [38,39] (original values).

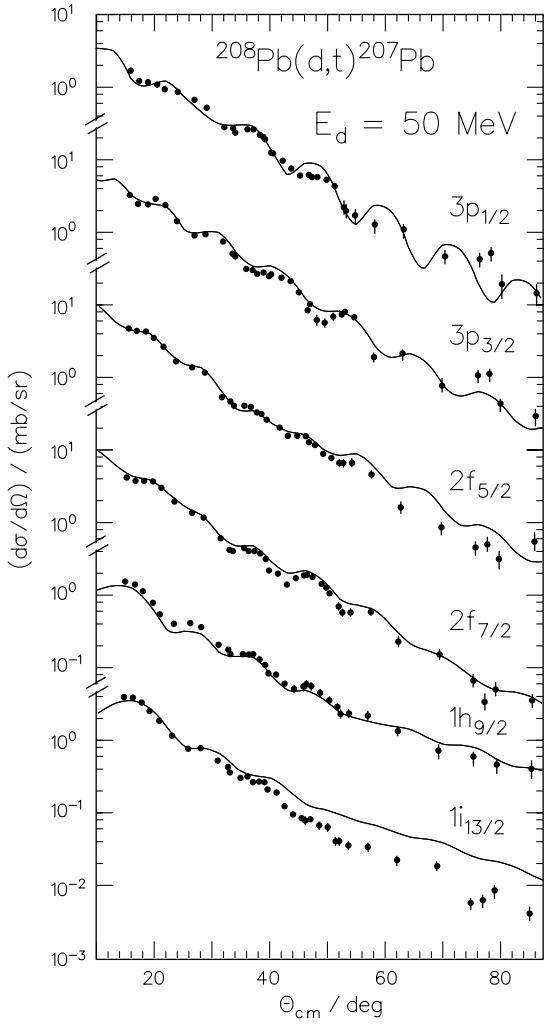

Fig. 5. Angular distributions of differential cross-sections from the ^{208}Pb(d,t)^{207}Pb reaction at 50 MeV (ref. [40]) are compared to DWBA calculations.

from ref. [38,39] and single-particle wave functions derived from the potentials described in section 4. The quality of the fits is comparable to that obtained in the original work.

The spectroscopic factors deduced with the usually adopted methods are on the average 20% smaller than the shell model expectation value $S = 1$, see table 3. They are larger than those of the previous analysis at the same beam energy and they are in better agreement with spectroscopic factors deduced from other (d,^{3}He) experiments performed at different deuteron energies and from (t,α) reactions, compare, *e.g.*, the compilation given in ref. [39].

5.2 The ^{208}Pb(d,t)^{207}Pb reaction

For the reanalysis of the neutron pick-up experiments we took the (d,t) data measured by Parkinson *et al.* [40] at 50 MeV and the (p,d) data measured by Whitten *et al.* [41] at 22 MeV. Both are recommended by the Nuclear Data Sheets [22] for their spectroscopic results. In fig. 5 the angular distributions of the differential cross-section for the (d,t) reaction of ref. [40] are shown and compared to the new DWBA calculations. The agreement is regarded as being satisfactory.

Table 4. Spectroscopic factors S from the (d,t) and (p,d) reactions on ^{208}Pb.

$E_x{}^{(a)}$	$J^{\pi(a)}$	S(d,t)$^{(b)}$	S(d,t)$^{(c)}$	S(p,d)$^{(d)}$	S(p,d)$^{(e)}$
0.0	$1/2^-$	0.79	0.95	0.66	1.10
0.570	$5/2^-$	0.79	0.82	0.76	0.67
0.898	$3/2^-$	0.67	0.88	0.68	1.00
1.633	$13/2^+$	0.70	0.92	0.68	0.46
2.340	$7/2^-$	0.70	0.86	0.74	0.42
3.416	$9/2^-$	0.91	0.74	0.55	0.22

$^{(a)}$ Energies in MeV, ref. [22].
$^{(b)}$ This work, data from ref. [40].
$^{(c)}$ Reference [40] (original values).
$^{(d)}$ This work, data from ref. [41].
$^{(e)}$ Reference [41] (original values).

The numbers given in table 4 allow the comparison between the spectroscopic factors for pick-up from the $3p_{1/2}$, $2f_{5/2}$, $3p_{3/2}$, $1i_{13/2}$, $2f_{7/2}$ and $1h_{9/2}$ neutron shells obtained from the original analyses of the (d,t) and the (p,d) reaction and those from the reanalysis with the wave functions calculated in the effective potentials described in section 4. The spectroscopic factors from the present analysis of the (d,t) reaction are smaller by 25% than the shell model expectation value and they are smaller than the original numbers. The new spectroscopic factors for the (p,d) reaction [41] are systematically smaller by 30% than the shell model expectation value, whereas the original numbers scatter noticeably around the value $S = 1$. From the combined reanalysis of the (d,t) and (p,d) data we obtain an average spectroscopic factor $S = 0.72$.

5.3 The ^{208}Pb(^{3}He,d)^{209}Bi reaction

The proton particle states have been investigated among others by Wildenthal *et al.* [42]. The angular distributions of deuterons corresponding to stripping into the $1h_{9/2}$, $2f_{7/2}$, $1i_{13/2}$, $3p_{3/2}$, $2f_{5/2}$ and the $3p_{1/2}$ proton shells are shown in fig. 6. We notice a fair agreement with the new DWBA calculations. The corresponding spectroscopic factors are given in table 5. The original values are distributed around the shell model value of $S = 1$ with a 10% scatter. The reanalysis of these data relies on the more standard spin orbit strength $\lambda_{\rm DW} = 12$ instead of a value of $\lambda_{\rm DW} = 6$ used in the original work [42]. This yields sizable differences to the original results with a maximum deviation of 57% from $S = 1$, however, the same trend of depletion with increasing excitation energy is found as seen in the present analysis with the new potentials. The calculations with the new wave functions give reasonable results only for the ground-state transition ($S = 0.83$) (table 5, column 3). The other particle states, which are

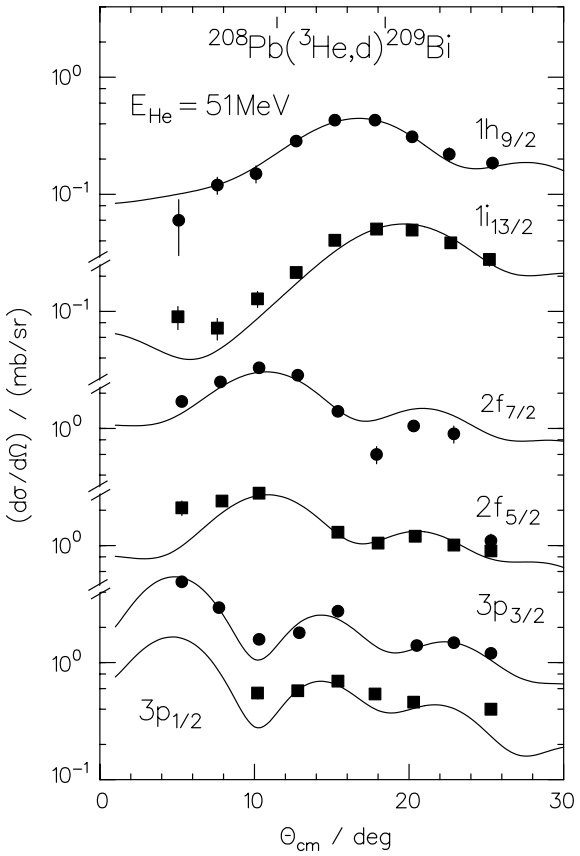

Fig. 6. Angular distributions of differential cross-sections from the ^{208}Pb(^{3}He,d)^{209}Bi reaction at 51.26 MeV (ref. [42]) are compared to DWBA calculations.

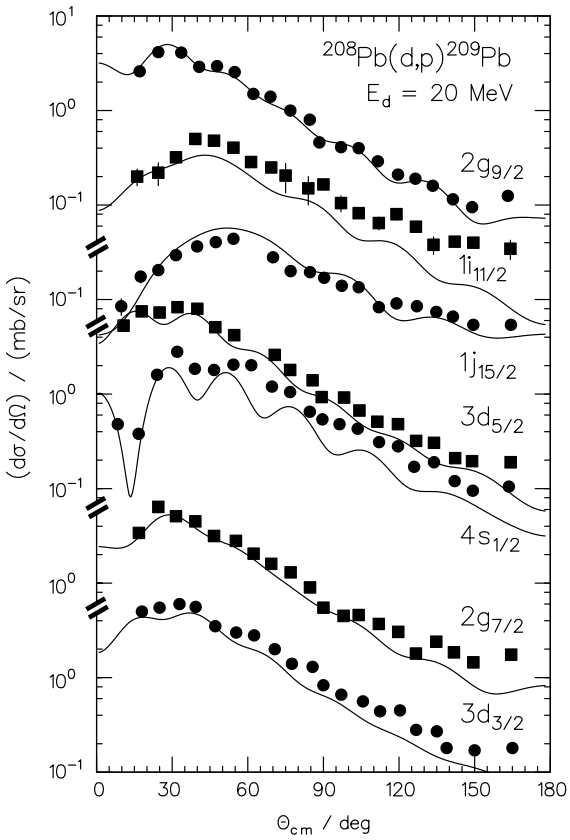

Fig. 7. Angular distributions of differential cross-sections from the ^{208}Pb(d,p)^{209}Pb reaction at 20 MeV (ref. [43]) are shown with DWBA predictions.

Table 5. Spectroscopic factors S from the ^{208}Pb(^{3}He,d)^{209}Bi reaction at 51.26 MeV.

E_x [a]	J^π [a]	S [b]	S [c]	S [d]
0.0	$9/2^-$	0.83	1.00	1.19
0.896	$7/2^-$	0.33	1.12	0.99
1.609	$13/2^+$	0.45	0.94	0.96
2.826	$5/2^-$	0.28	1.14	0.85
3.120	$3/2^-$	0.13	1.08	0.43

[a] Energies in MeV, ref. [21].
[b] This work, data from ref. [42].
[c] Reference [42] (original values).
[d] Reanalysis of data from ref. [42] with $\lambda_{\rm DW} = 12$.

weakly bound, show decreasing spectroscopic factors with increasing excitation energy. This might have experimental reasons, because these states are known to be fragmented to some extent, and possibly other (unbound) fragments could have been missed in the experiments. Another explanation can be found in the validity of our wave functions, since the corresponding single-particle energies, which constitute the basis of the potential fitting procedure, were taken in the calculations with larger errors, *i.e.* with lower weights, in view of the comparably unclear experimental situation.

5.4 The ^{208}Pb(d,p)^{209}Pb reaction

Among the (d,p) reactions quoted in the Nuclear Data Sheets [22] we selected the data of Kovar *et al.* [43] taken at deuteron energies of 20 MeV and those of Muellehner *et al.* [44] taken at 25 MeV. In fig. 7 we show the proton angular distribution corresponding to stripping a neutron into the $2g_{9/2}$, $1i_{11/2}$, $1j_{15/2}$, $3d_{5/2}$, $4s_{1/2}$, $2g_{7/2}$ and the $3d_{3/2}$ shells. The agreement between the DWBA predictions including the new bound state wave functions and the experimental angular distributions is convincing. In table 6 we compare the spectroscopic factors from the original investigations of the (d,p) reaction with those obtained from our reanalysis.

The original spectroscopic factors from both experiments exhibit a remarkable scattering from $S = 0.58$ to $S = 1.17$ with an average value of $S = 0.95$. The numbers resulting from our reanalysis are generally smaller than the previous ones, and we obtain an average value of $S = 0.58$. The agreement between the new spectroscopic factors determined for both sets of data must be regarded as very satisfactory in view of the many error sources

Table 6. Spectroscopic factors S from the ^{208}Pb(d,p)^{209}Pb reaction at 20 MeV.

E_x [a] (MeV)	J^π [a]	S			
		(d,p) [b]	(d,p) [c]	(d,p) [d]	(d,p) [e]
0.0	$9/2^+$	0.47	0.83	0.39	0.67
0.779	$11/2^+$	0.68	0.86	0.61	0.94
1.423	$15/2^-$	0.35	0.58	0.43	1.13
1.567	$5/2^+$	0.54	0.98	0.68	1.00
2.032	$1/2^+$	0.66	0.98	0.77	0.93
2.491	$7/2^+$	0.53	1.05	0.55	1.17
2.538	$3/2^+$	0.56	1.07	0.83	1.17

[a] Reference [21].
[b] This work, data from ref. [43].
[c] Reference [43] (original values).
[d] This work, data from ref. [44].
[e] Reference [44] (original values).

associated with the reconstruction of the experimental data and the subsequent fitting procedure.

5.5 Occupation numbers

In a comparative consideration of the results obtained from a reanalysis of selected data from proton and neutron pick-up and stripping experiments on ^{208}Pb we see that the measured angular distributions can be reproduced by DWBA calculations with the new bound state wave functions with a quality comparable to the original "best fits". The use of a complete set of wave functions left no room to tamper the absolute and the relative spectroscopic factors. Considering this aspect the corresponding values exhibit a comparatively small scatter around a mean value of $S = 0.74$ for proton and neutron hole states and a mean value of $S = 0.59$ for particle states (except the excited states of ^{209}Bi, where experimental problems are imaginable). Averaged over pick-up and stripping data we obtain a mean value of $S = 0.67$. This result is remarkable, because very similar numbers were obtained from an analysis of (e,e′p) reactions [45] and from theoretical considerations including short-range correlations of the nuclear many-body system [1,46,47].

5.6 Nucleon densities and rms radii

The possibility of another test of the new wave functions represents the comparison of calculated mean-field densities for protons and neutrons with measured charge and mass densities and with densities calculated within different models. The densities for (point) protons and neutrons shown in fig. 8 were obtained by a summation of the single particle densities deduced from our wave functions with the respective statistical weight $(2j+1)$ including all nucleons up to the Fermi energy.

The results are in qualitative agreement with charge densities measured in elastic electron scattering on

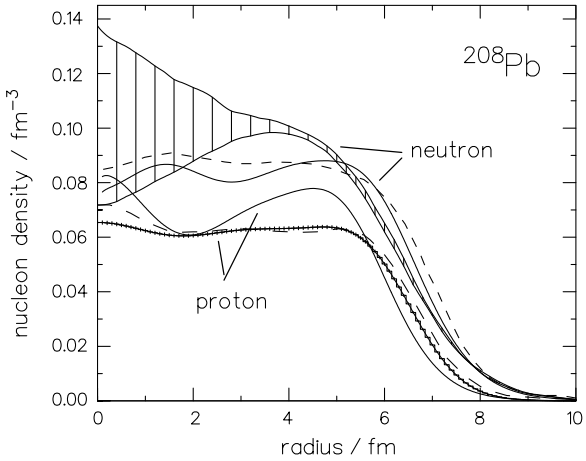

Fig. 8. Mean-field densities for neutrons and protons (full lines) as determined from the complete set of wave functions calculated with the state-independent potentials of section 4 are compared to measured densities of refs. [25,48] (vertical hatching to indicate experimental uncertainties) and results of relativistic Hartree calculations (ref. [32], dashed lines).

Table 7. rms radii in fm for point proton and neutron densities of ^{208}Pb.

Reference	Proton	Neutron
Present	5.224	5.735
[48]	5.453	5.611
[33]	5.46	5.73
[32]	5.469	5.721

^{208}Pb [25] and neutron densities deduced from the measured mass distribution [26,48]. The present proton density is smaller and the neutron density extends to larger radii; however note the uncertainties of the experiments, which are indicated by the hatched area in fig. 8. We compare the densities with predictions from a relativistic Hartree calculation [32] which are in quite good agreement for neutrons. For protons the Hartree calculation is in better agreement with the experimental data than the density from the sums of present wave functions. A nearly perfect agreement shows the comparison with the mean-field neutron density and with that obtained from relativistic Hartree calculations [33]. Good agreement with measured charge density was obtained by, *e.g.*, Hasse *et al.* [49] and Jaminon *et al.* [50] in mean-field calculations when the occupation probabilities were adjusted.

The respective numerical values for the rms radii are given in table 7 for the total (point) densities and in table 8 for some orbitals close to the Fermi surface. The second data set originates from early low-energy nucleon transfer experiments [51–55] analysed in local and non-local DWBA approximation and with the assumption of full spectroscopic strength $S = 1$ in these shells. Columns 4 and 8 give model predictions and show a general agreement. Similar as in case of the total density, the rms

Table 8. rms radii in fm for neutron and proton orbitals in ^{208}Pb.

Proton				Neutron			
$n\ell_J$	Present	Exp.	Theory	$n\ell_J$	Present	Exp.	Theory
$1h_{9/2}$	5.638	6.10 [51]	6.08 [53]	$3p_{1/2}$	6.394	6.10 [54]	6.15 [55]
$3s_{1/2}$	5.419	5.25 [52]	5.37 [53]	$2f_{5/2}$	6.196	5.92 [54]	6.05 [55]
$2d_{3/2}$	5.481	5.39 [52]	5.51 [53]	$3p_{3/2}$	6.322	5.97 [54]	6.1 [55]
$1h_{11/2}$	5.827	6.08 [52]	6.22 [53]	$2f_{7/2}$	6.177	5.76 [54]	
$2d_{5/2}$	5.498	5.37 [52]	5.49 [53]	$1i_{13/2}$	6.437	6.20 [54]	
				$1h_{9/2}$	5.843	5.90 [54]	

radii of the present work are smaller than the predictions, whereas the neutron rms radii are predicted reasonably well on average. There is also access to single-particle densities via magnetic electron scattering. However, as small admixtures of other components, the so-called core polarisation, easily affect the measured cross-sections, we do not discuss these results.

6 Discussion of the spin-orbit splitting

In a very detailed investigation Scheerbaum [20] has tried to describe quantitatively the observed spin-orbit splittings on the basis of the Brueckner-Hartree-Fock theory. He has shown, that in lowest-order perturbation theory, the spin-orbit splitting of a valence nucleon outside a spin-saturated core arises entirely from the spin-orbit part of the nucleon-nucleon interaction, and there are no contributions from the tensor force and the quadratic spin-orbit force. With a complete treatment of the direct and the exchange part of the spin-orbit interaction, Scheerbaum calculated the contribution of spin-saturated shells to the spin-orbit splitting for neutrons:

$$\varepsilon_{\rm so}(n\ell) = \big(2\ell{+}1\big)\frac{\pi}{3}S^{30}\int_0^\infty \frac{1}{r}\frac{\mathrm{d}}{\mathrm{d}r}\Big(\rho_{\rm p}{+}2\rho_{\rm n}\Big)R^2(n\ell)\cdot r^2\mathrm{d}r. \tag{9}$$

S^{30} characterizes the strength of the triplet-odd part of the nucleon-nucleon interaction, $\rho_{\rm p}$ and $\rho_{\rm n}$ are proton and neutron densities. The spin-orbit splitting for protons is given by interchange of $\rho_{\rm p}$ and $\rho_{\rm n}$ in eq. (9). An estimate for the complete splittings in ^{208}Pb is rendered more difficult due to the unknown influence of the spin-unsaturated $1h$ proton and $1i$ neutron shells. Scheerbaum has shown, that a calculation with realistic nucleon-nucleon interactions, harmonic oscillator wave functions $R^2(n\ell)$ and model densities $\rho_{\rm p}$ and $\rho_{\rm n}$ yields values of $\varepsilon_{\rm so}$, which are far too small in comparison to the experiment.

We tried another interpretation of eq. (9). Inserting the radial wave functions $R^2(n\ell)$ and the single-particle densities of the spin-saturated shells, calculated from the wave functions in the state-independent potential (section 4), one can take S^{30} as a parameter to reproduce the absolute measured values of $\varepsilon_{\rm so}(n\ell)$. These can be reproduced with a mean value of $S^{30} = (-59{\pm}6)$ MeVfm^5 for neutrons and of $S^{30} = (-52 \pm 3)$ MeVfm^5 for protons. This result should be compared to $S^{30} = -46.3$ MeVfm^5 for the Yale potential and with $S^{30} = -47.4$ MeVfm^5 for the Gammel-Thaler potential. Obviously, a nearly quantitative description of the spin-orbit splittings can be achieved. The contribution of the spin-unsaturated shells, however, remains unclear.

Instead of calculated densities, one can introduce measured proton and neutron densities in eq. (9), tacitly including the spin-unsaturated $1h_{11/2}$ proton and $1i_{13/2}$ neutron shells. But the quality of the description of $\varepsilon_{\rm so}(n\ell)$ with deduced strength parameters $S^{30} = (-53 \pm 7)$ MeVfm^5 for neutrons and $S^{30} = (-50 \pm 7)$ MeVfm^5 for protons is not so convincing.

Scheerbaum [20] also tried to give an estimate of the contribution of the tensor interaction to the nuclear spin-orbit splitting:

$$\varepsilon_{\rm so}(n\ell) = -(2\ell+1)\ K_{\rm T}\int_0^\infty \frac{\rho}{r}\frac{\mathrm{d}\rho}{\mathrm{d}r}\ R^2(n\ell)\cdot r^2\mathrm{d}r\,. \tag{10}$$

These matrix elements contain a radial form factor, which is quite similar to that of eq. (9). Inclusion of the tensor part of the nucleon-nucleon interaction in our analysis, however, could not improve the fit of $\varepsilon_{\rm so}(n\ell)$ obtained from eq. (9) with pure spin-orbit interaction.

An investigation of the single-particle spin-orbit potential exceeding the work of Scheerbaum has been performed by Penzel and Stocker [11]. In addition to the direct part of the spin-orbit potential they treat explicitly the exchange part up to second order. For the calculation of the spin-orbit matrix elements they use harmonic oscillator wave functions and give predictions for $\varepsilon_{\rm so}(n\ell)$ in case of $N = Z$ nuclei with spin-saturated shells. They find that the first-order contributions to the splittings of levels near the Fermi energy (results of Scheerbaum) are reduced by an amount of about 30% due to the second-order contributions. For a hypothetic $N = Z$ nucleus with $A = 208$ they obtain values of $\varepsilon_{\rm so}(n\ell)$ which are quite similar to those found in ^{208}Pb. They can also describe qualitatively the empirically found reduction of $\varepsilon_{\rm so}$ with increasing n for given ℓ-values. The role of spin-unsaturated shells remains, however, unexplained.

The attempts of Bhattacharya [9] to describe the observed spin-orbit splittings with a spin-orbit potential derived from a Woods-Saxon potential with adapted

geometry were not successful. He describes neither the absolute values of ε_{so} with the desired accuracy, nor the fine-structure of ε_{so}, expressed by the dependence on the principal quantum number n. The ratio $\tilde{\varepsilon}(1h)/\tilde{\varepsilon}(2d) = 1.27$ for protons, for example, is by far too small compared to the observed value of 1.90. The failure of a quantitative description is, however, not astonishing in view of the simplicity of the model.

Single-particle energies in ^{208}Pb were calculated by Belgoumène *et al.* [13] in an average field of Woods-Saxon type and with a spin-orbit term constructed in a self-consistent manner from the single-particle densities. This leads to a reduction of adjustable parameters compared to methods usually applied. As a result the energies for protons and neutrons in ^{208}Pb are fairly well described and the level ordering is in general reproduced, but a correct description of the fine structure $\varepsilon_{so}(n\ell)$ is missing.

Calculations in the frame of a relativistic mean-field model with derivative couplings were performed by Chiapparini *et al.* [12] for finite nuclei, as, *e.g.*, ^{208}Pb. The shape of the resulting central and spin-orbit potentials show certain similarities with the pure phenomenological potentials from the present paper. Because this theoretical investigation only aims at a principal understanding of nuclear phenomena, a quantitatively correct description of the single-particle energies cannot be expected. Indeed, the absolute agreement between measured and calculated energies is little satisfactory.

7 Concluding remarks

Many experiments and related theoretical investigations have shown, that properties of few selected nuclei can be described in the frame of the simple shell model. Such nuclei are found near closed shells and ^{208}Pb was thought to be the most important candidate. The basic strong spin-orbit splitting could be qualitatively described in the past as result of the spin-orbit term, and other components of the free nucleon-nucleon interaction or, alternatively, in the frame of the solution of the relativistic many-body problem of finite nuclei. A quantitatively correct description of the measured phenomena is, however, still missing. For practitioners therefore it seems worthwhile to look for an effective nuclear and spin-orbit potential, which both describe in a pure phenomenological model the experimental properties of the nuclei. In order to avoid model assumptions whenever possible, the construction by the model should be guided in a consistent way by the requirement to use only measured data for input.

We succeeded in finding potentials individually shaped to reproduce the single-particle energies for protons and neutrons in ^{208}Pb, *e.g.* the energetic position of the low-lying states in ^{207}Tl, ^{207}Pb, ^{209}Bi and ^{209}Pb. The sole assumption was that the nuclear central potential and the spin-orbit potential are mutually connected by the Thomas prescription. This connection can be explained theoretically [20] and seems to be at least plausible. The resulting potentials are local and state independent. They represent effective potentials, in which all known and possibly unknown effects are incorporated. The spin-orbit potential, *e.g.*, contains all contributions resulting from the spin-orbit-, tensor- and quadratic spin-orbit parts of the nucleon-nucleon interaction.

The validity of the two complete sets of proton and neutron wave functions was tested successfully in the frame of a detailed reanalysis of spectroscopic results from single-particle transfer reactions on ^{208}Pb. The corresponding spectroscopic factors show no ambiguities; their absolute, mean value amounts to $S = 0.67$ in accordance with other experimental [1,39] and theoretical [46,47] results. Proton and neutron densities derived from the new wave functions by summing all contributions from the occupied orbits could be compared successfully with measured densities. They could be also used to calculate spin-orbit splittings in the frame of the Scheerbaum model. As a result, we arrived at a consistent description of all relevant available spectroscopic data.

References

1. V.R. Pandharipande, I. Sick, P.K.A. de Witt Huberts, Rev. Mod. Phys. **69**, 981 (1997).
2. P. Grabmayr, G. Mairle, U. Schmidt-Rohr, Phys. Bl. **55**, 35 (1999).
3. A. Bohr, B. Mottelson, *Nuclear Structure* (Benjamin, New York, 1969).
4. C. Mahaux, R. Sartor, Adv. Nucl. Phys. **20**, 1 (1991).
5. G. Mairle, Phys. Lett. B **304**, 39 (1993).
6. G. Mairle, Z. Phys. A **350**, 285 (1995).
7. E. Rost, Phys. Lett. B **26** 184 (1968).
8. J. Blomquist, S. Wahlborn, Ark. Fys. **16**, 545 (1960).
9. R. Bhattacharya, Z. Phys. A **322**, 665 (1985); **327** 31 (1987).
10. W. Stocker, Nucl. Phys. A **159**, 222 (1970).
11. R. Penzel, W. Stocker, Nucl. Phys. A **190**, 218 (1972).
12. M. Chiapparini, A. Delfino, M. Malheiro, A. Gattone, Z. Phys. A **357**, 47 (1997) and references given therein.
13. B. Belgoumène, J. Dudek, T. Werner, Phys. Lett. B **267** 431 (1991).
14. J.D. Walecka, Ann. Phys. **83**, 491 (1974).
15. J. Zimanyi et al., Phys. Rev. C **42**, 1416 (1990); Nucl. Phys. A **484**, 647 (1988).
16. W. Koepf, M.M. Sharma, P. Ring, Nucl. Phys. A **533**, 95 (1991).
17. M.M. Sharma, S.A. Moszkowski, P. Ring, Phys. Rev. C **44**, 2493 (1991).
18. C.H. Blanchard, R. Avery, Phys. Rev. **81**, 35 (1951).
19. R.J. Blin-Stoyle, Philos. Mag. **46**, 973 (1955).
20. R.R. Scheerbaum, Phys. Lett. B **61** 151 (1970); Nucl. Phys. A **257**, 77 (1976); Phys. Lett. B **63** 381 (1976).
21. M.J. Martin, Nucl. Data Sheets **63**, 726 (1991).
22. M.J. Martin, Nucl. Data Sheets **70**, 315 (1993).
23. K.L.G. Heyde, *The Nuclear Shell Model* (Springer Verlag, Heidelberg, 1994).
24. M. Rejmund, M. Schramm, K.H. Maier, Phys. Rev. C **59**, 2520 (1999).
25. B. Frois et al., Phys. Rev. Lett. **38**, 152 (1977); B. Frois, private communication.

26. L. Ray, P.E. Hodgson, Phys. Rev. C **20**, 2403 (1979).
27. G. Eder, H. Oberhummer, Lett. Nuovo Cimento **15**, 609 (1976).
28. M. Ermer, PhD thesis, Tübingen University, 1990; M. Ermer, H. Clement, P. Grabmayr, G. Graw, R. Hertenberger, H. Kader, G.J. Wagner, J. Phys. (Paris), Colloque, C **6**, 431 (1990).
29. M. Brack, *Ecole International Joliot-Curie de Physique Nucléaire* (1992), p. 325.
30. M. Waroquier, Hoger Aggregaatsthesis (1982), Gent, unpublished.
31. R.D. Lawson, *Theory of the Nuclear Shell Model* (Clarendon Press, Oxford, 1980).
32. B.A. Nikolaus, T. Hoch, D.G. Madland, Phys Rev. C **46**, 1757 (1992).
33. C.J. Horowitz, B.D. Serot, Nucl. Phys. A **368**, 503 (1981).
34. P. Ring, E. Werner, Nucl. Phys. A **211**, 198 (1973).
35. K. Saito, K. Tsushima, A.W. Thomas, Nucl. Phys. A **609**, 39 (1996).
36. P.D. Kunz, computer code DWUCK4, private communication.
37. P. Grabmayr et al., Phys. Lett. B **164**, 516 (1985).
38. P. Grabmayr, G.J. Wagner, H. Clement, H. Röhm, Nucl. Phys. A **494**, 244 (1989).
39. P. Grabmayr, Prog. Part. Nucl. Phys. **29**, 251 (1992).
40. W.C. Parkinson, D.L. Hendrie, H.H. Duhm, J. Mahoney, J. Saudinos, G.R. Satchler, Phys. Rev. **178**, 1976 (1969).
41. C.A. Whitten, N. Stein, G.E. Holland, D. Bromley, Phys. Rev. **188**, 1941 (1969).
42. B.H. Wildenthal, P.M. Preedom, E. Newman, M.R. Cates, Phys. Rev. Lett. **19**, 960 (1967).
43. D.G. Kovar, N. Stein, C. Bockelmann, Nucl. Phys. A **231**, 266 (1974).
44. G. Muehllehner, A.S. Poltorak, W.C. Parkinson, R.H. Bassel, Phys. Rev. **159**, 1039 (1967).
45. E. N. M. Quint et al., Phys. Rev. Lett. **58**, 1086 (1987).
46. V. Pandharipande, C. Papanicolas, J. Wambach, Phys. Rev. Lett. **53**, 1133 (1984).
47. S. Fantoni, V.R Pandharipande, Nucl. Phys. A **427**, 473 (1984).
48. L. Ray, Phys. Rev. C **19**, 1855 (1979).
49. R.W Hasse, B.L. Friman, D. Berdichevsky, Phys. Lett. B **181**, 5 (1986).
50. M. Jaminon, C. Mahaux, H. Ngo, Nucl. Phys. A **440**, 228 (1985).
51. A. Warwick, R. Chapman, J.L. Durell, J.N. Mo, J. Kuehner, Nucl. Phys. A **356**, 33 (1981).
52. P.W. Woods, R. Chapman, J.N. Mo, P. Skensved, J. Kuehner, Phys. Lett. B **116**, 320 (1982).
53. D.W.L. Sprung, J. Martorell, X. Campi, Nucl. Phys. A **268**, 301 (1976); and citations in references [51] and [52].
54. H.J. Körner, J.P. Schiffer, Phys. Rev. Lett. **27**, 1457 (1971).
55. E. Friedman, D. Nir, D. Sueaqui, Y. Tuchman, Phys. Rev. C **9**, 2340 (1974).